Article title: The honeysuckle genome provides insight into the molecular mechanism of carotenoid metabolism underlying dynamic flower coloration

Authors: Xiangdong Pu, Zhen Li, Ya Tian, Ranran Gao, Lijun Hao, Yating Hu, Chunnian He, Wei Sun, Meimei Xu, Reuben J. Peters, Yves Van de Peer, Zhichao Xu, Jingyuan Song
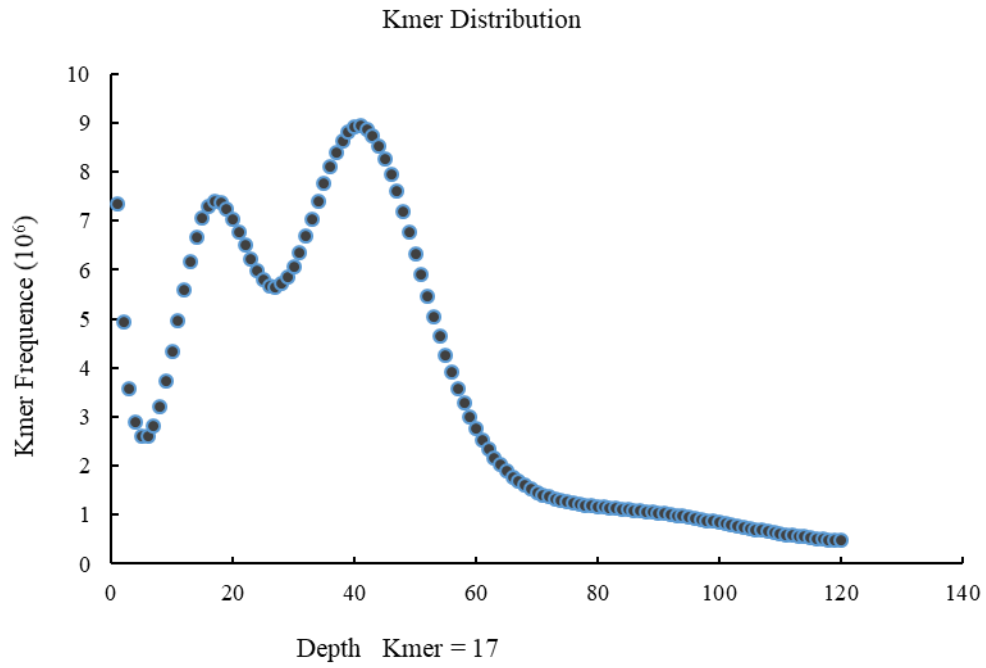
Figure S1. *L. japonica* genome survey using 17 k-mer distribution analysis, indicating high heterozygosity.
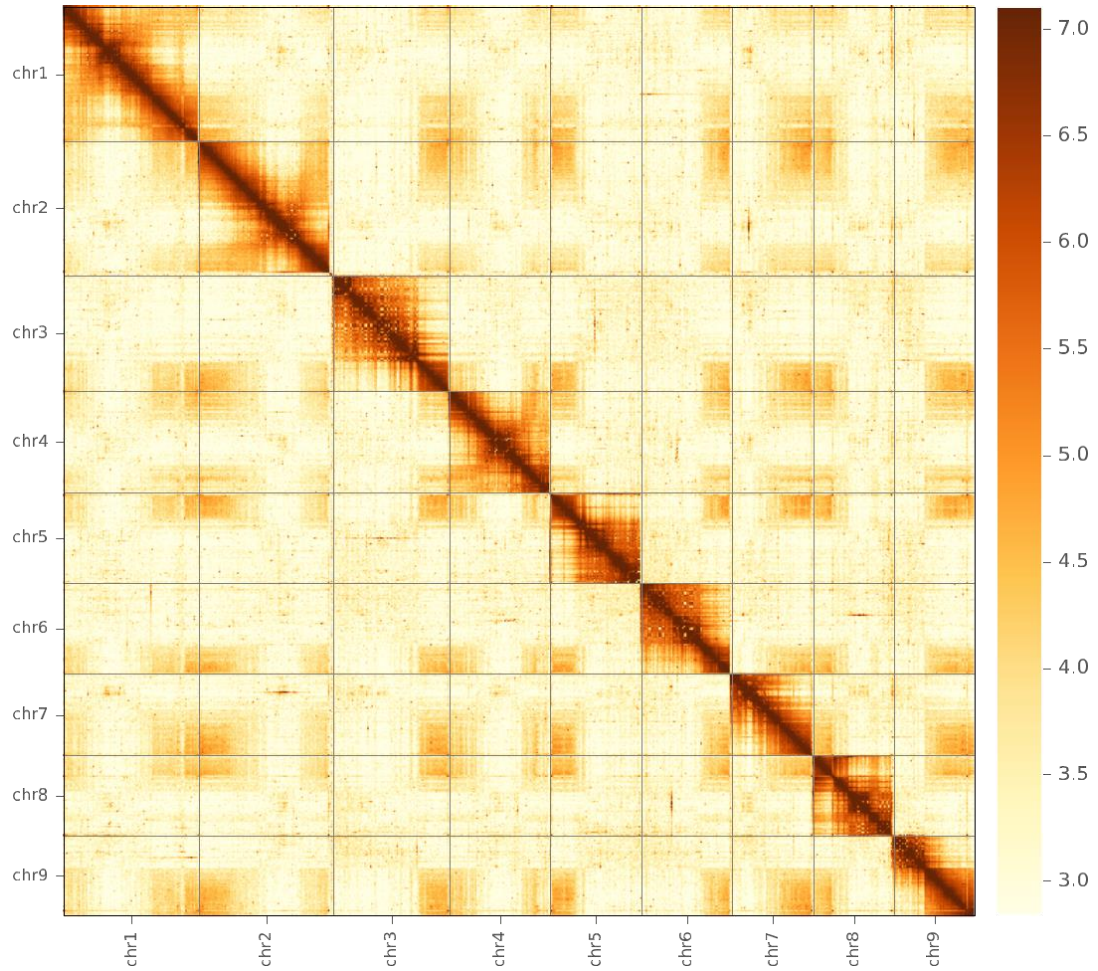
Figure S2. Hi-C intra-chromosomal contact map for the genome assembly (2n=18) using LACHESIS.
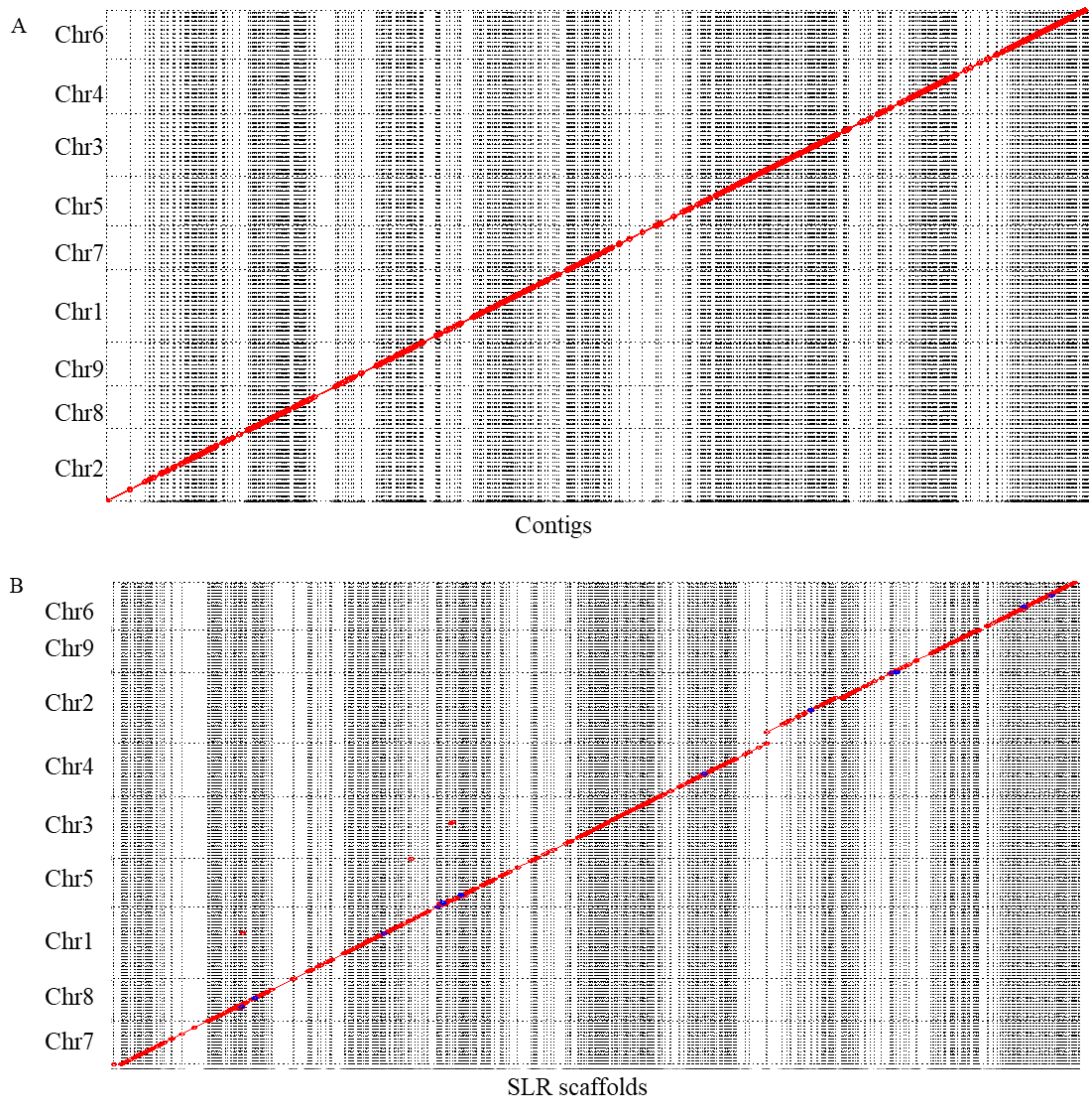
Figure S3. A. The contigs were anchored into nine chromosomes using LACHESIS. B. The SLR scaffolds were assembled based on ONT reads and contig assembly, and then were aligned to the chromosomal assembly.
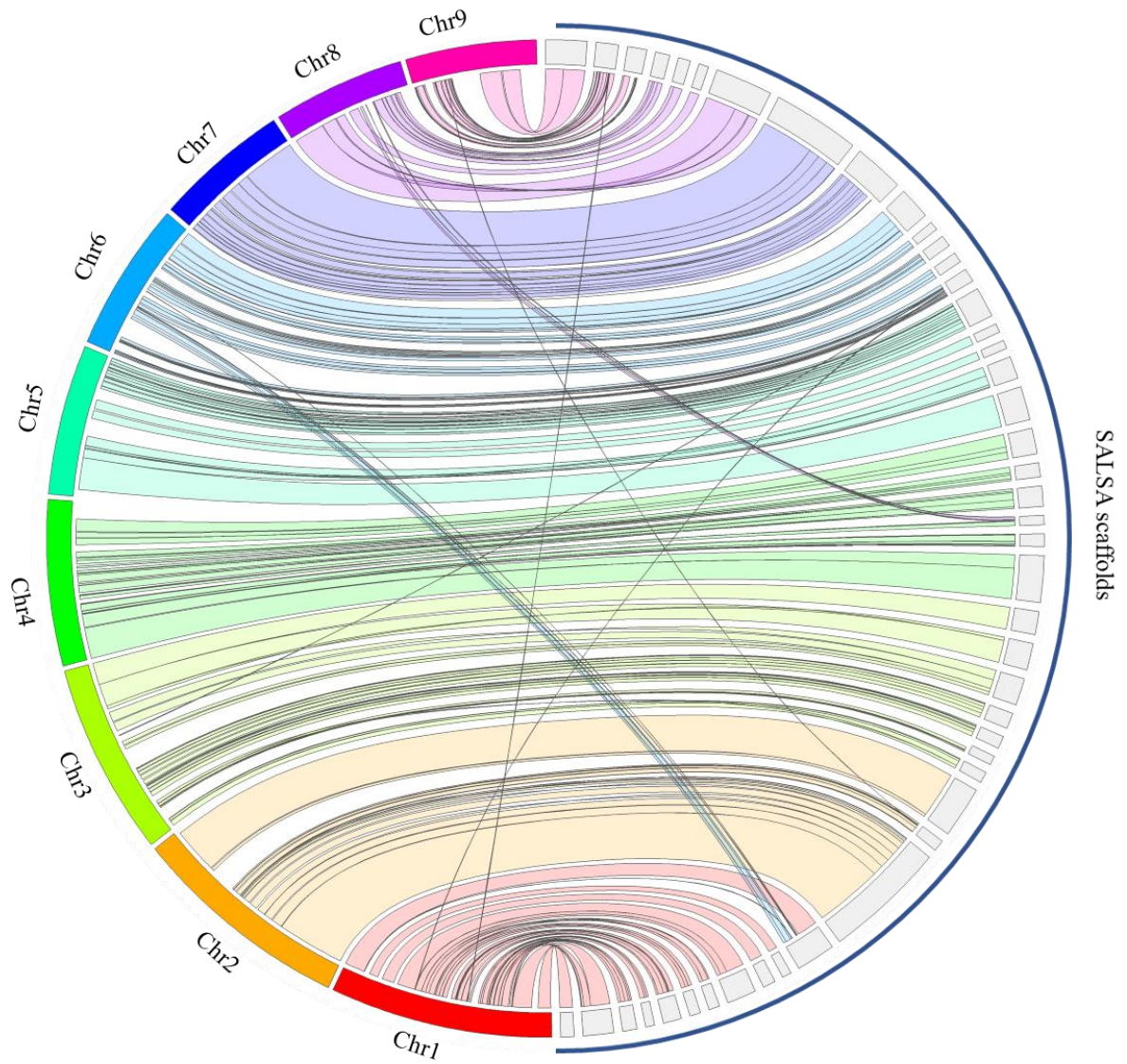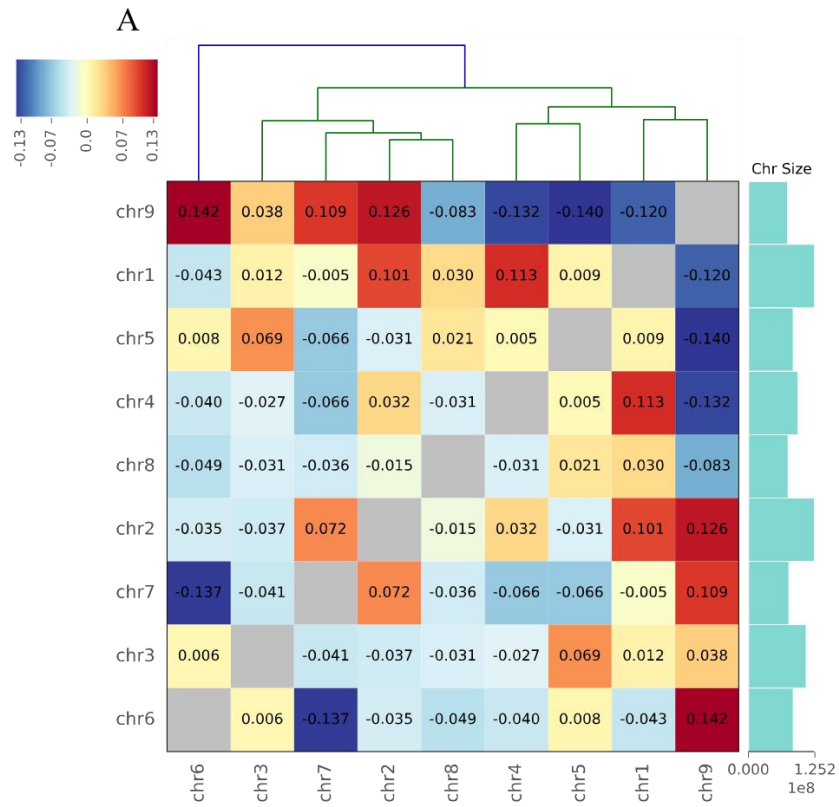
Figure S4. The alignment between chromosomal assembly and SALSA scaffolds (SALSA). The SALSA scaffolds were assembled based on Hi-C data. A total of 46 SALSA scaffolds, covering 75% genome size, accurately aligned to the chromosomal assembly.
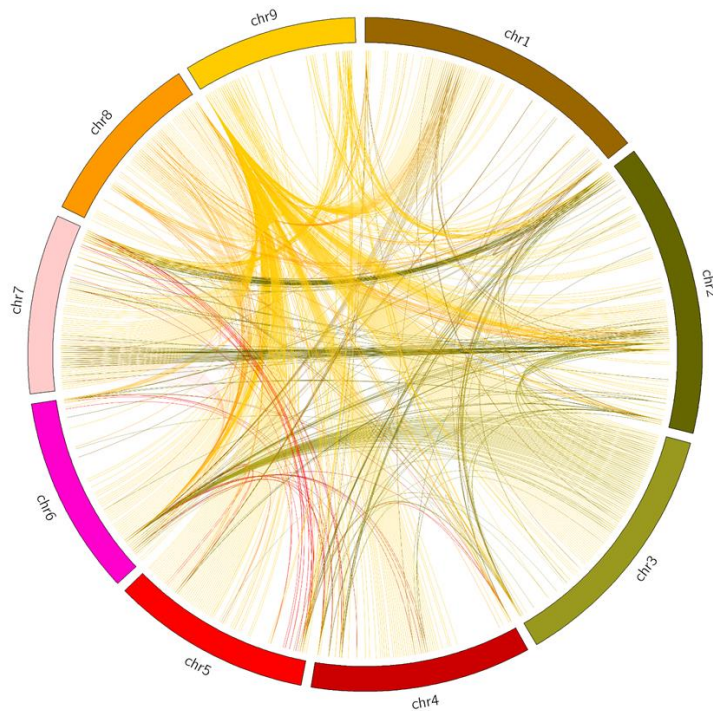
Figure S5. The expected number of contacts between all whole chromosome pairs (A) and circos plot of 1,000 bin pairs (B) showing inter-chromosomal interactions.
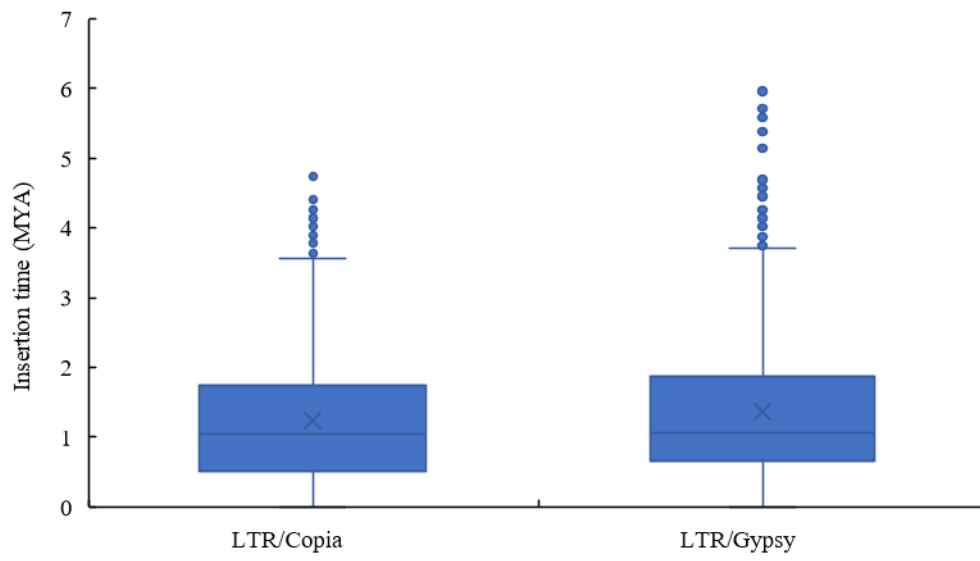
Figure S6. Insertion times of LTR/*Copia* and LTR/*Gypsy* retrotransposons in the *L. japonica* genome. The horizontal lines indicate the median value. The blue circles indicate the outliers.
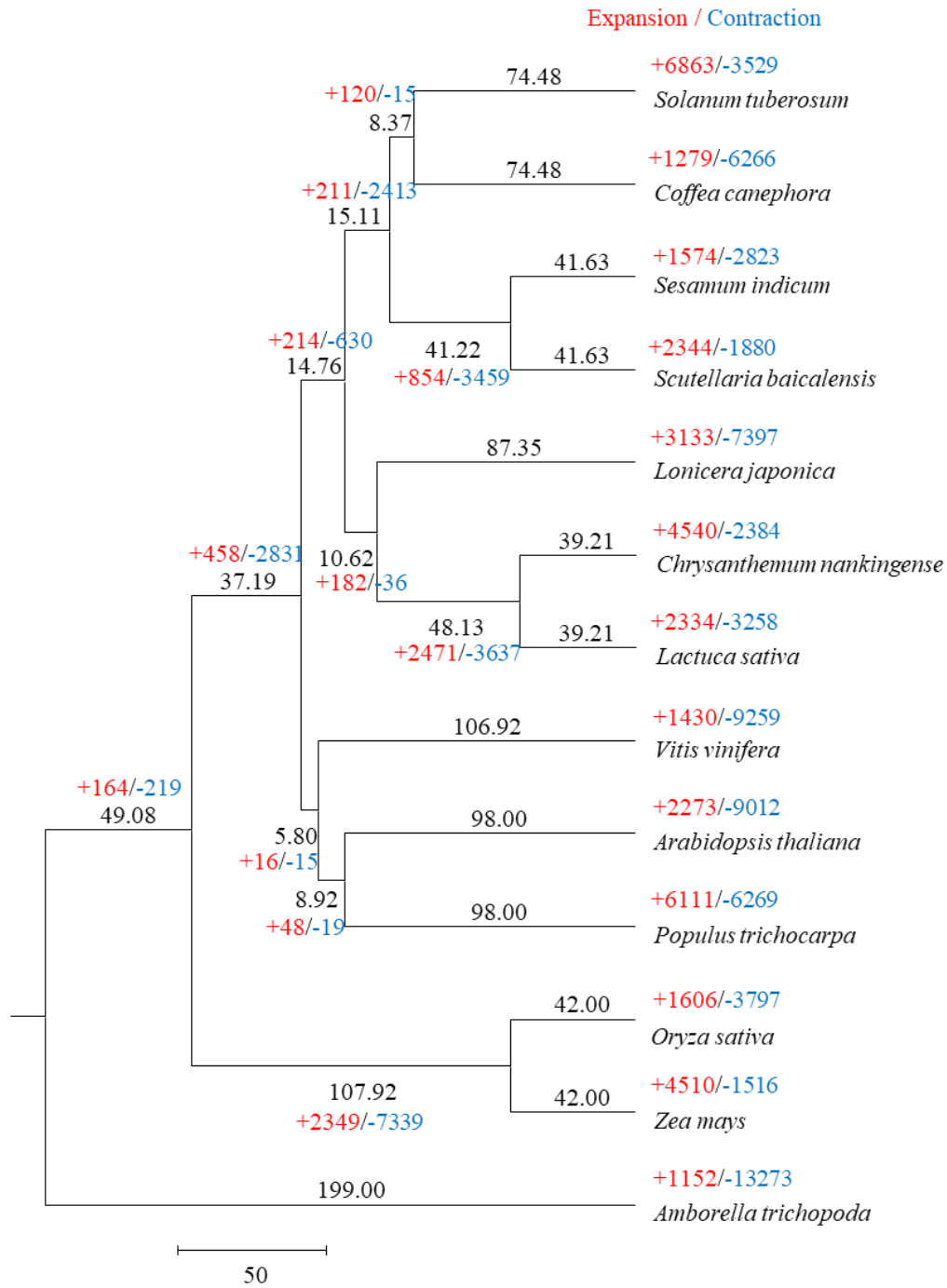
Figure S7. Expansion and contraction of gene families within 13 plant species.
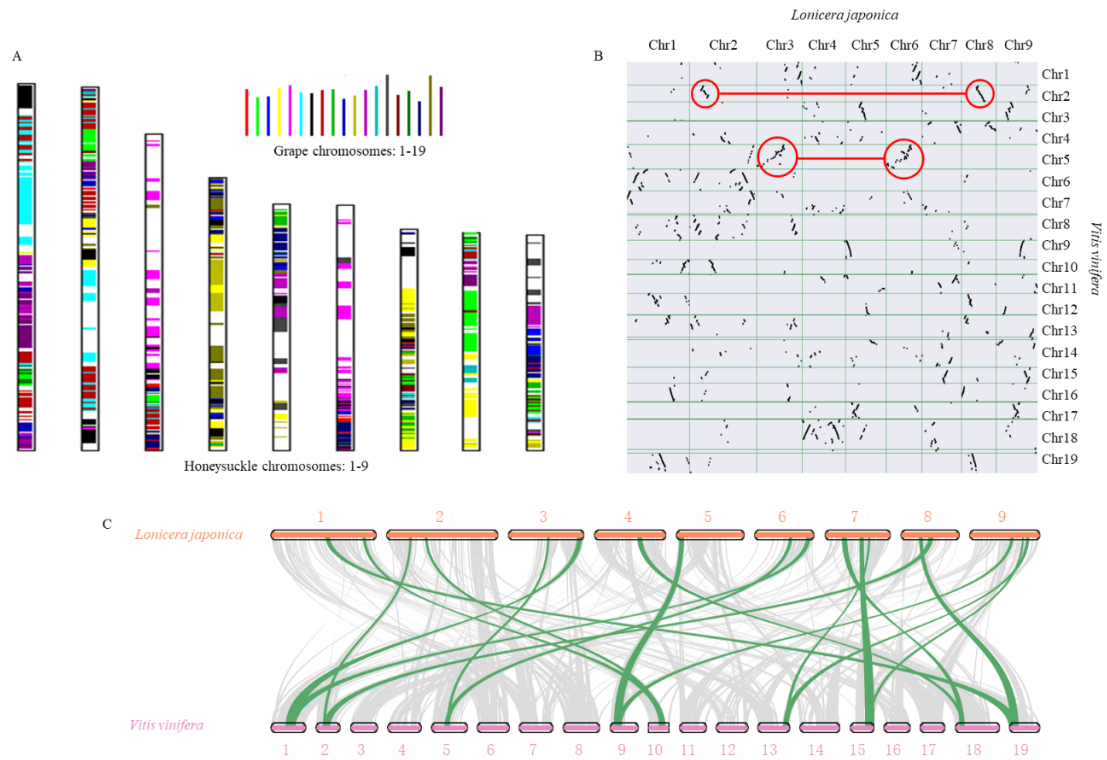
Figure S8. Synteny analysis between *L. japonica* and grape (*Vitis vinifera*) genomes. A. Genome painter showing gene collinearity between the *L. japonica* and grape genomes. B. Dot plot displaying synteny between *L. japonica* and grape genomes. Red circles highlight a *L. japonica* genome duplication event. C. Macrosynteny visualization between *L. japonica* and grape karyotypes. Green lines present two *L. japonica* syntenic blocks that correspond to one grape block.
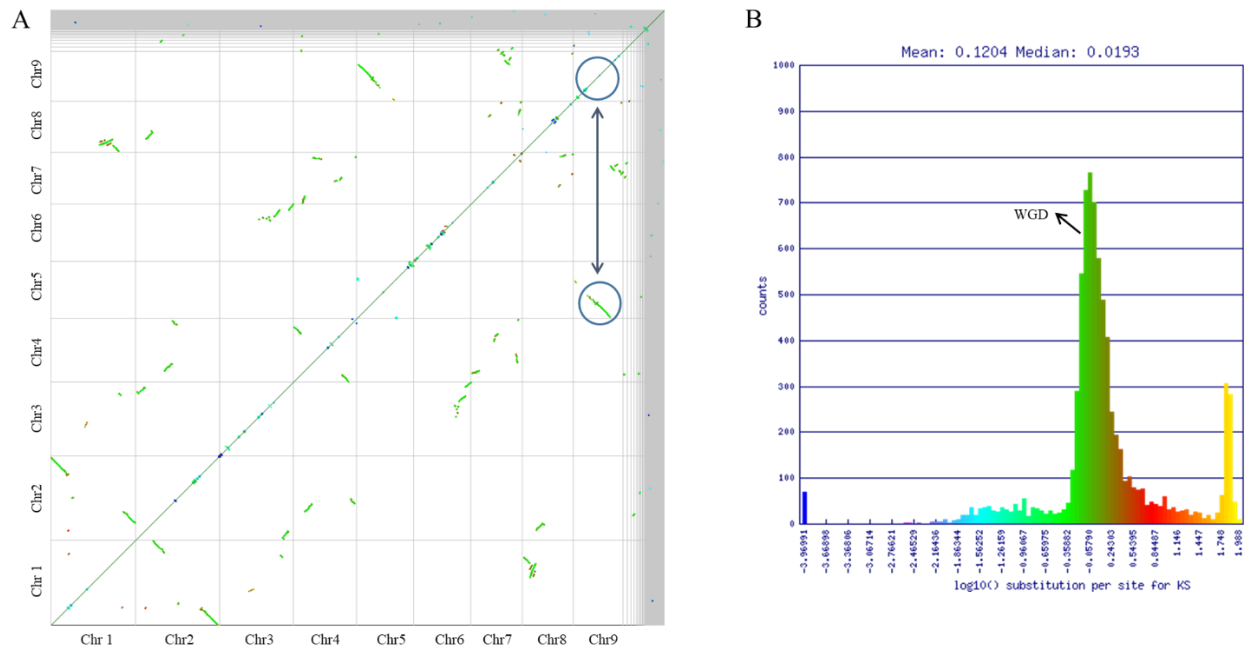
Figure S9. A. The synteny of *L. japonica* paralogous gene pairs by synmap2 of the CoGe pipeline. The green plot represents the duplication of large fragments. B. The K_S value of *L. japonica* paralogous gene pairs. The maximum DAGChainer distance between two matches is 120kb.
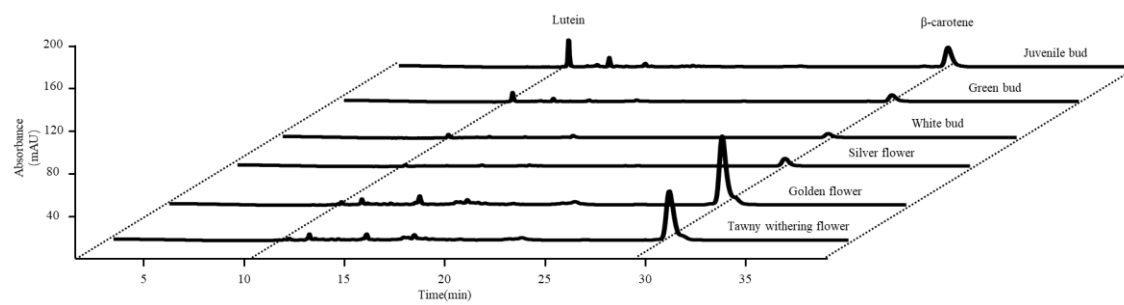
Figure S10. UPLC analysis of carotenoids at different flower developmental stages. Lutein and β-carotene are the two main compounds at different flower developmental stages.
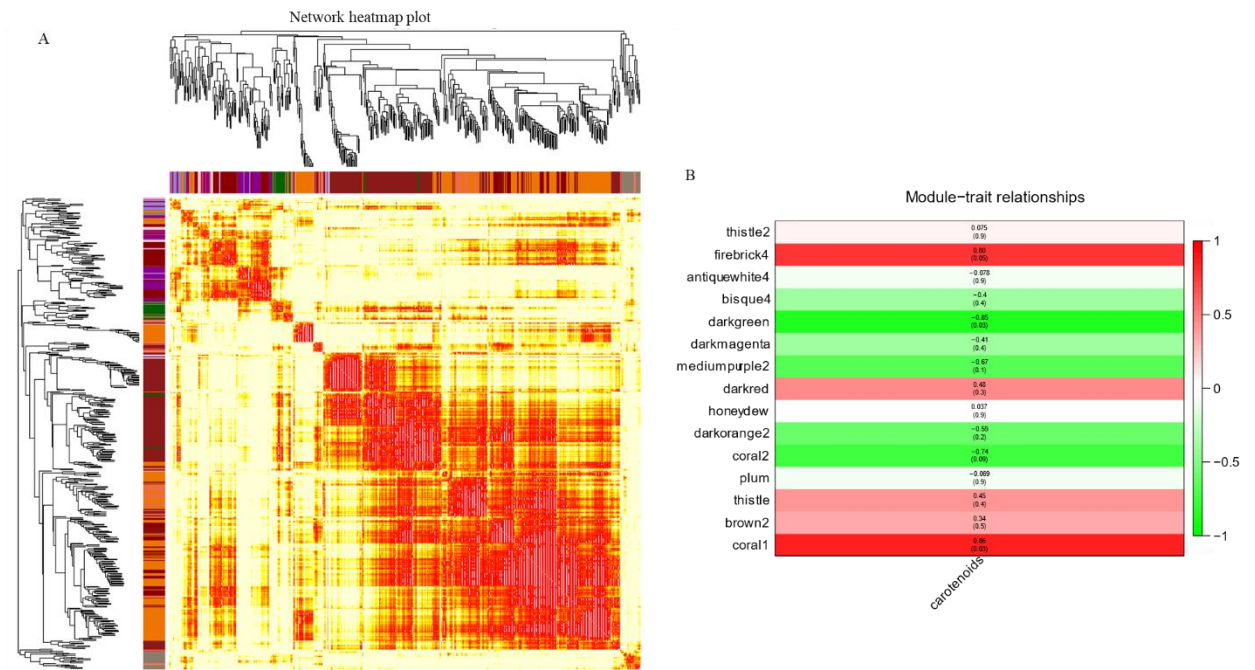
Figure S11. WGCNA network analysis and connection with carotenoid contents at different flower stages. A. Hierarchical cluster tree and relationship between gene co-expression modules (heatmap). B. Module-trait corrections and corresponding *P*-values. The trait represented carotenoid content at different flower stages.
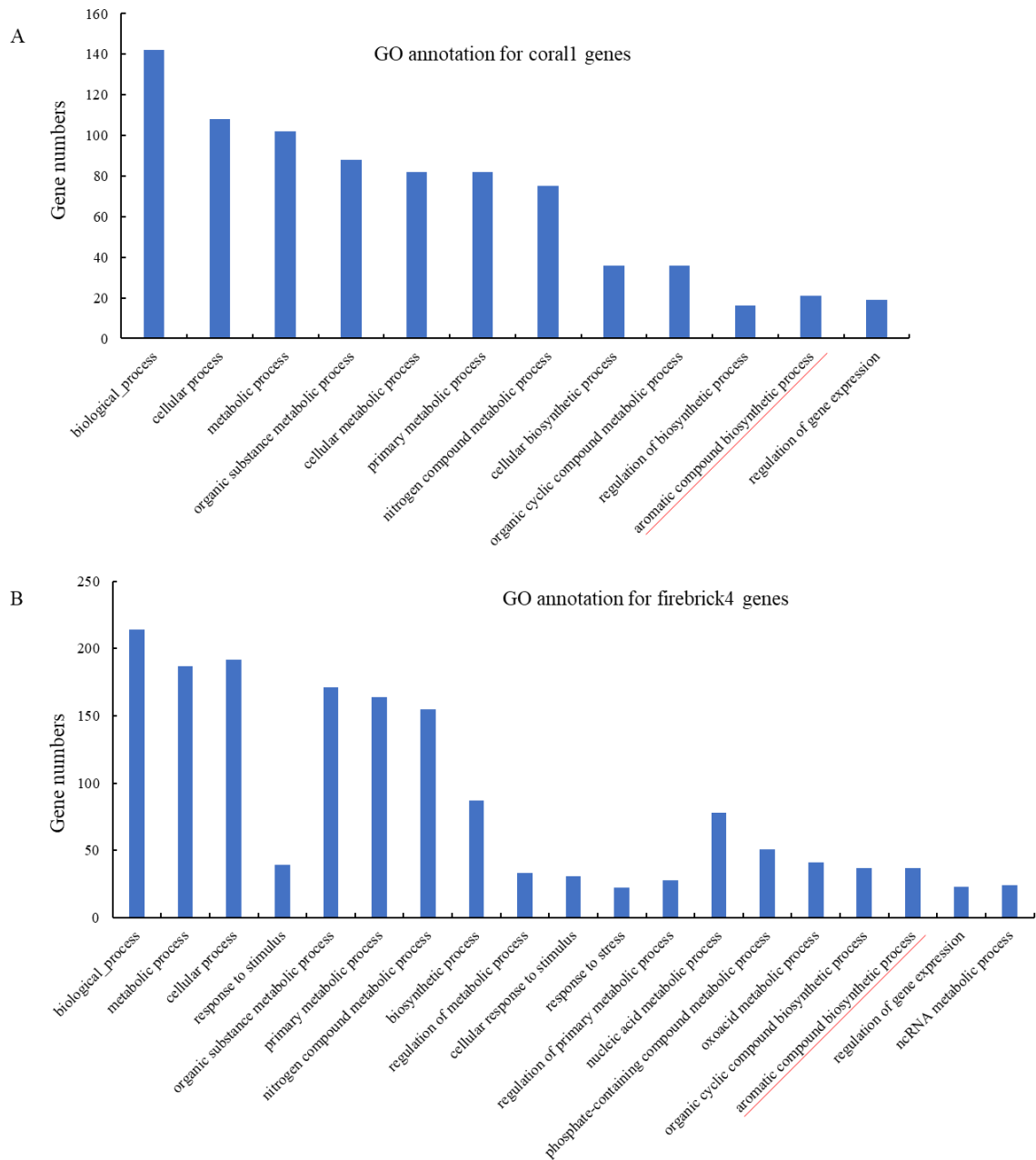
Figure S12. Gene ontology (GO) annotation of 'coral1' module genes (A) and 'firebrick4' module genes (B).
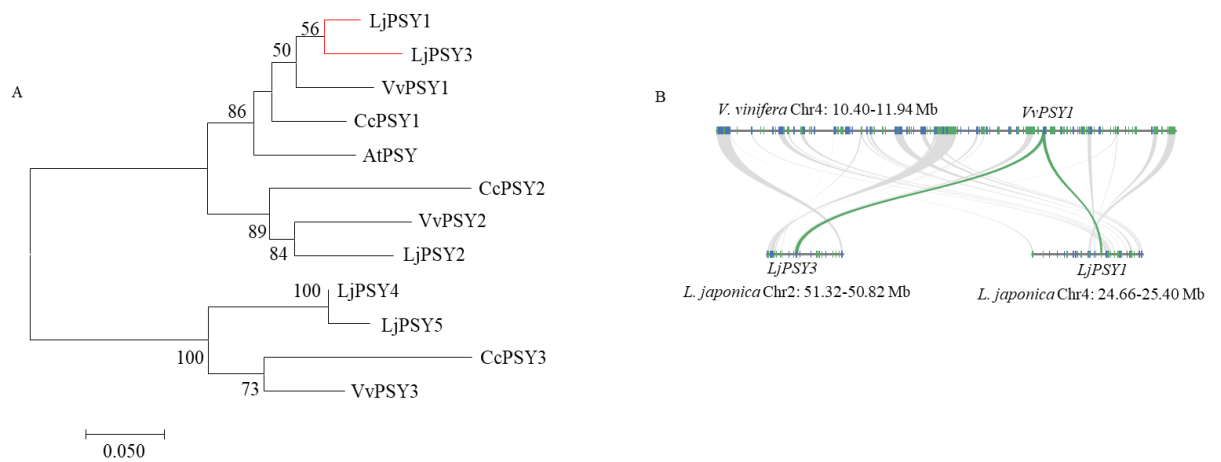
Figure S13. Evolutionary analysis of PSY genes. A. ML tree for PSY genes from *L. japonica*, *C. canephora*, *V. vinifera* and *A. thaliana*: LjPSY1 (Lj4C251T7), LjPSY2 (Lj8C97G11), LjPSY3 (Lj2C511G6), LjPSY4 (Lj2C707G6), LjPSY5 (Lj2A718G15), VvPSY1 (GSVIVT01035255001), CcPSY1 (Cc00_g26180), VvPSY2 (GSVIVT01020828001), CcPSY2 (Cc08_g11740), VvPSY3 (GSVIVT01025421001), CcPSY3 (Cc01_g02520), AtPSY (AT5G17230). B. Gene synteny analysis between *L. japonica* and *V. vinifera*. The syntenic block with *VvPSY* seems to correspond to two blocks containing *LjPSY1* and *LjPSY3*.
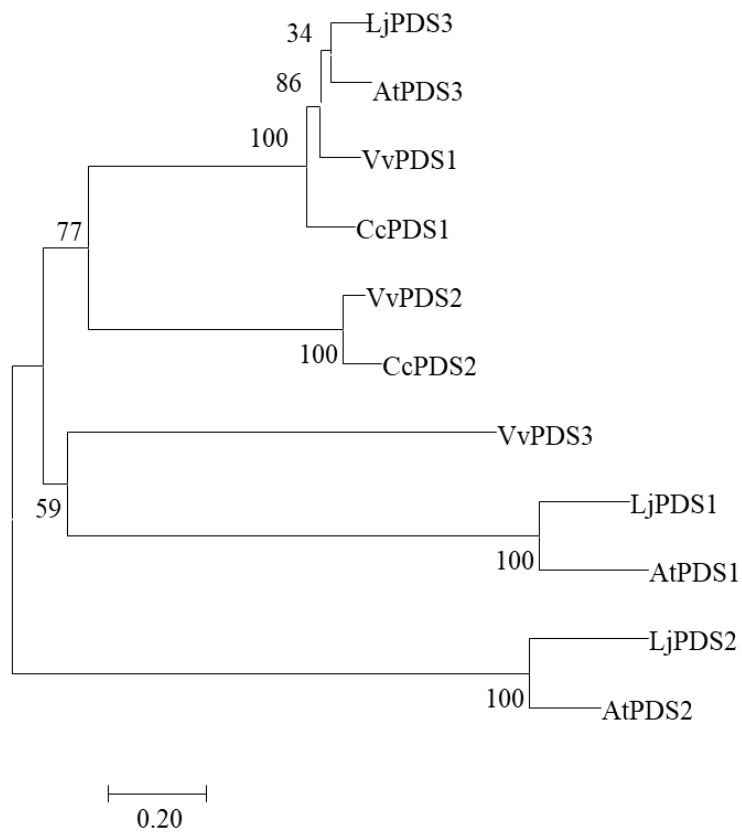
Figure S14. Evolutional analysis of PDS genes. ML tree for PDS genes from *L. japonica*, *C. canephora*, *V. vinifera*, and *A. thaliana*: LjPDS1 (Lj8C8T1), LjPDS2 (Lj2C359T6), LjPDS3 (Lj9A539T91), VvPDS1 (GSVIVT01016650001), VvPDS2 (GSVIVT01021843001), VvPDS3 (GSVIVT01023990001), CcPDS1 (Cc04_g00540), CcPDS2 (Cc02_g31750), AtPDS1 (AT1G06570), AtPDS2 (AT3G11945), AtPDS3 (AT4G14210).
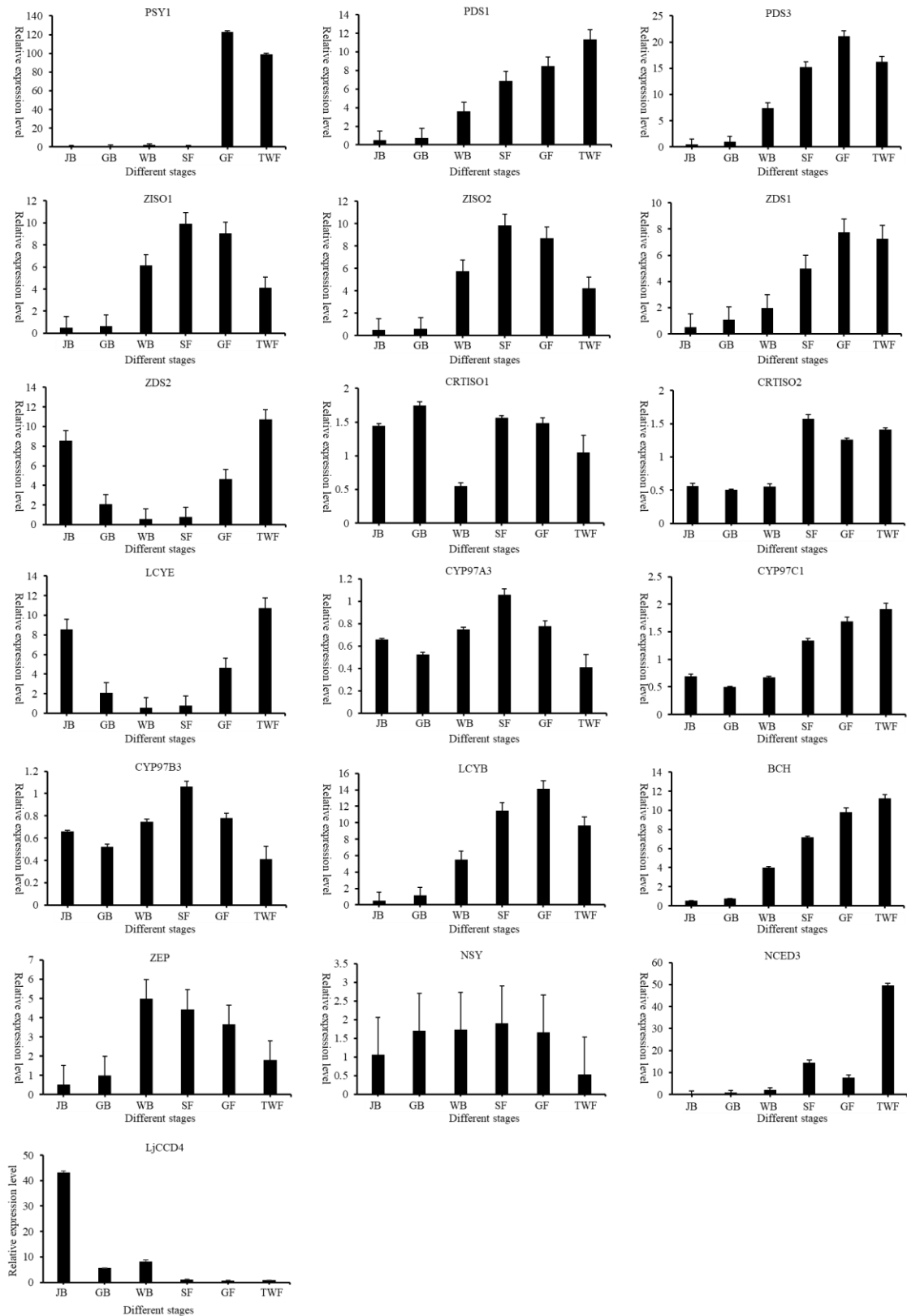
Figure S15. Gene expression analysis by qPCR at different flower developmental stages. Juvenile bud, JB. Green bud, GB. White bud, WB. Silver flower, SF. Golden flower, GF. Tawny withering flower, TWF. Error bars represent standard deviation obtained from three biological repeats.
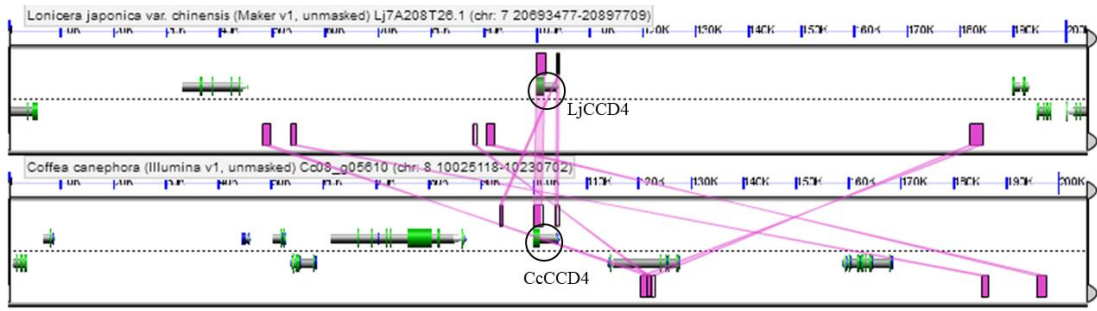
Figure S16. Synteny of CCD4 genomic regions between *L. japonica* and *C. canephora*.
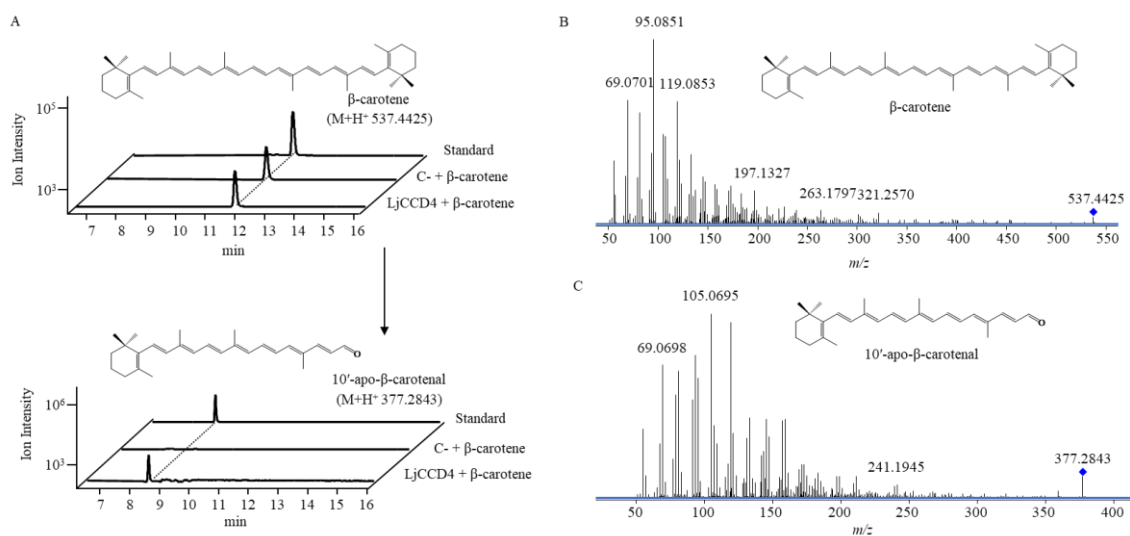
Figure S17. Functional characterization of LjCCD4 incubated with β-carotene. A, LC-MS chromatogram of *in vitro* reactions performed with crude enzyme from *E. coli* transformed with empty pET-32a vector (C−) or LjCCD4 (LjCCD4) expression vector. B, MS/MS analysis of β-carotene. C, MS/MS analysis of 10′-Apo-β-carotenal.
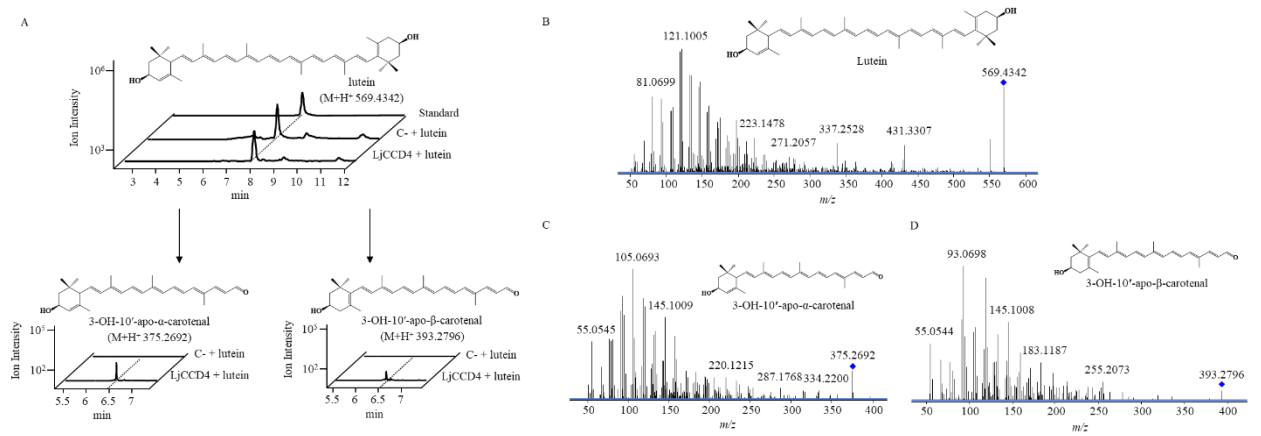
Figure S18. Functional characterization of LjCCD4 incubated with lutein. A, LC-MS chromatogram of the *in vitro* reactions performed with crude enzyme from *E. coli* transformed with empty pET-32a vector (C−) or LjCCD4 (LjCCD4) expression vector. B, MS/MS analysis of lutein. C, MS/MS analysis of 3-OH-10′-Apo-α-carotenal. D, MS/MS analysis of 3-OH-10′-Apo-β-carotenal.
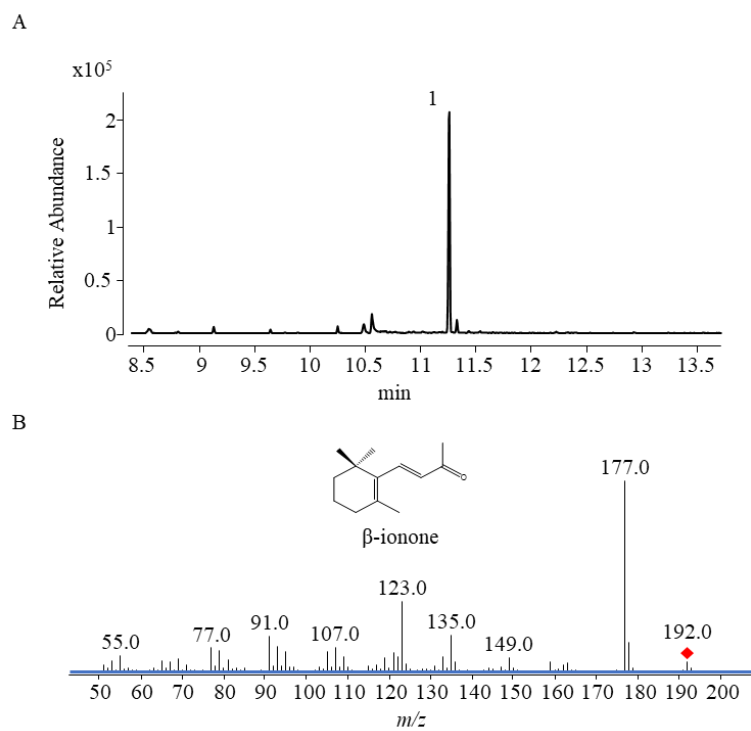
Figure S19. GC–MS analysis of LjCCD4 incubated with β-carotene. A, GC-MS analysis of the products. B, MS/MS analysis of β-ionone (1).
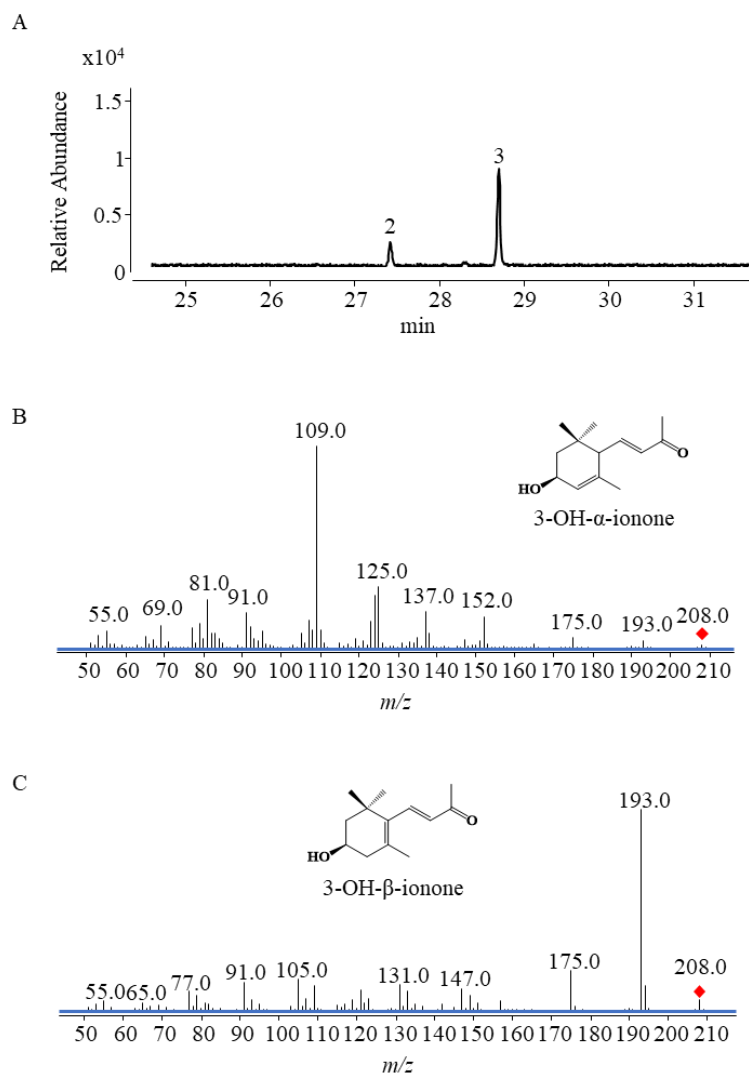
Figure S20. GC–MS analysis of LjCCD4 incubated with lutein. A, GC-MS analysis of the products. B, MS/MS analysis of 3-OH-α-ionone (2). C, MS/MS analysis of 3-OH-β-ionone (3).
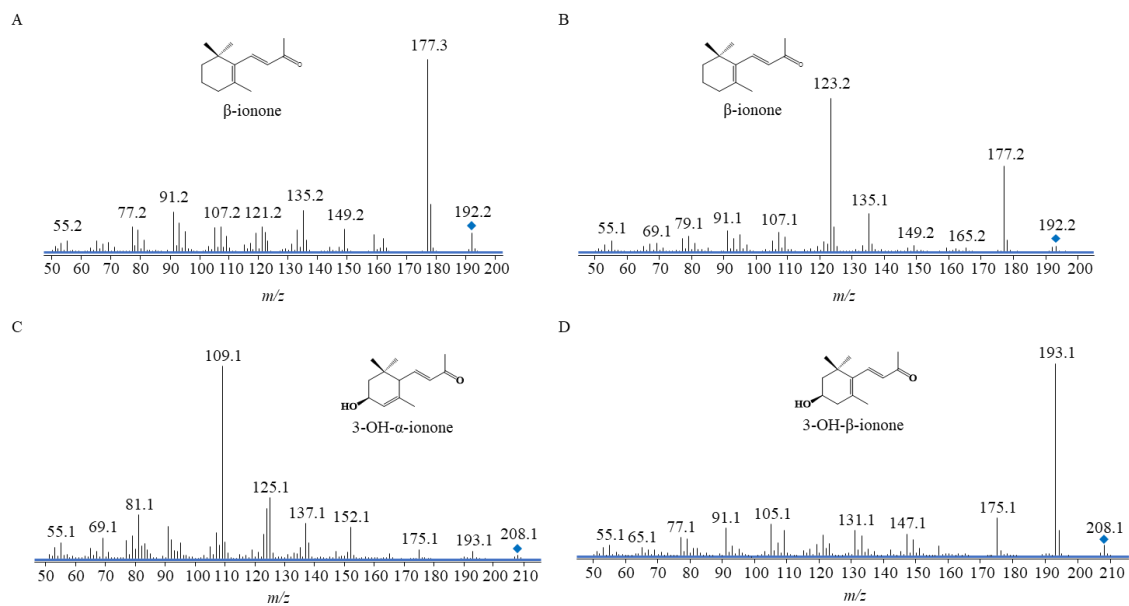
Figure S21. GC–MS analysis of LjCCD1b incubated with A, 10′-Apo-β-carotenal. B, β-carotene. C and D, lutein.